Fabrication of mesoporous titania membrane of dual-pore system and its photocatalytic activity and dye-sensitized solar cell performance

2011 Nanotechnology 22 275309

(http://iopscience.iop.org/0957-4484/22/27/275309)

Nanotechnology **22** (2011) 275309 (7pp) doi:10.1088/0957-4484/22/27/275309

Fabrication of mesoporous titania membrane of dual-pore system and its photocatalytic activity and dye-sensitized solar cell performance

Seung-Lim Oh[1,2], Kyong-Hoon Choi[1], Ji-Eun Im[1], Kang-Kyun Wang[1], Hae-Yong Yaung[3], Kyungkon Kim[3] and Yong-Rok Kim[1,4]

[1] Department of Chemistry, Yonsei University, Seoul 120-749, Republic of Korea
[2] Gangneung Center, Korea Basic Science Institute, Gangneung 210-702, Republic of Korea
[3] Solar Cell Center, Energy Division, Korea Institute of Science and Technology (KIST), Seoul 136-791, Republic of Korea

E-mail: yrkim@yonsei.ac.kr

Received 23 December 2010, in final form 2 May 2011
Published 25 May 2011
Online at stacks.iop.org/Nano/22/275309

Abstract

We report the fabrication of a novel titania membrane of the dual-pore system that is strategically designed and prepared by a two-step replication process and sol–gel reaction. The primary nanoporous channel structure is fabricated by the cage-like PMMA template (CPT) obtained from the nanoporous alumina membrane and the secondary mesoporous structure is formed by the sol–gel reaction of the lyotropic precursor solution within the CPT. Furthermore the mesoporous titania membrane (MTM) frame consists of the titania nanoparticles of 10–12 nm in diameter. Morphology and structural properties of the MTM are investigated by field emission scanning electron microscopy, high resolution transmission electron microscopy, x-ray diffraction and Brunauer–Emmett–Teller surface area. The photocatalytic activity and the solar energy properties of the MTM are characterized by UV–vis spectrophotometer, spectrofluorometer and photoinduced I–V measurement. The photocatalytic test indicates that the MTM has higher efficiency than the commercial P25 with a good recyclability due to its large-scale membrane style and the preliminary result on the solar cell application shows a solar energy conversion efficiency of 3.35% for the dye-sensitized solar cell utilizing the MTM.

(Some figures in this article are in colour only in the electronic version)

1. Introduction

During the last decade, nanostructured titania materials have attracted much attention for important applications such as environmental purification, solar energy conversion, hydrogen production, photoconduction and molecular sensing due to their unique photophysical properties induced by the quantum size and the surface effect [1–5]. Among these applications, the photocatalytic degradation of organic pollutants and the dye-sensitized solar cell have become one of the most interesting fields [6–9]. To obtain the maximum efficiency for these applications, various nanostructured titania materials have also been fabricated in the direction of the reduced particle size and the increased surface area. In this regard, mesoporous titania has been a very interesting material due to its pore size tunability and the high specific surface area [10, 11]. Furthermore, the immobilization of titania composites as a film is more favored than the suspended powder type since the immobilization provides the recovery and the recycled usage.

Many research groups have reported the preparation of mesoporous titania nanopowders by the sol–gel method

[4] Author to whom any correspondence should be addressed.

through the surfactant-templated self-polymerization of titania [12, 13]. However, the powder type of titania has a problem in its retrieval. Generally the recycled usage is a very important factor in the industrial application. For this purpose, the fixing process of the mesoporous titania powders on the proper substrate is further needed by using the bonding chemicals [14–16]. But the bonding chemical buries most of the titania nanoparticles, leading to the decreased efficiency of photocatalytic activity. Therefore, in order to solve this problem, the highly ordered titania nanotube array film [17] and the titania nanotemplate [18] have been fabricated by anodizing methods with titanium foil. However, with respect to the specific surface area, the nanostructured titania materials still have a smaller area than the mesoporous titania nanopowders.

In this study, we report on the fabrication of the mesoporous titania membrane (MTM) that has well-ordered dual-pore arrays to maximize the specific surface area and maintain the surface quantum effect of nanoparticles. The photocatalytic activity and the dye-sensitized solar cell performance are evaluated to demonstrate the application potentials. The detailed structure of the MTM includes well-ordered pore arrays of the straight nanopore channels and the mesoporous walls between the nanopore channels that consist of the aggregated form of titania nanoparticles. The aggregated structure induces the mesoporosity that provides the large specific surface area.

2. Experimental details

2.1. Chemicals

High purity aluminum plate (Aldrich, 99.999%, 0.5 mm thick), phosphoric acid (Aldrich, 85%), copper(II) chloride dihydrate (Aldrich, $\geqslant$99.999%), hydrogen chloride (Aldrich, $\geqslant$99.7%), methyl methacrylate (MMA) (Aldrich, 99%), benzoyl peroxide (Sigma, $\sim$70%), sodium hydroxide (Aldrich, $\geqslant$98%), Pluronic F127 (BASF, $EO_{106}PO_{70}EO_{106}$) and titanium (IV) isopropoxide (Acros Organics, 98+%) were used without further purification.

2.2. Preparation of the MTM

The highly ordered nanoporous alumina membrane (nPAM) was utilized as a template. The nPAM was prepared by a two-step anodizing method with an aluminum plate (99.999%) [19]. The aluminum was anodized at a constant voltage of 180 V in 0.3 M phosphoric acid as an electrolyte at 0 °C for 12 h. After the anodization, the remaining aluminum substrate was removed by using a mixture solution of 0.2 M $CuCl_2$ and 6.0 M HCl. The barrier layer was then selectively removed by placing the nPAM in a 5.0 wt% phosphoric acid solution at 30 °C for 2 h. The obtained free-standing nPAM was rinsed with acetone and distilled water.

The nPAM with pore channels was inserted into the MMA monomer with 5.0 wt% benzoyl peroxide which was an initiator for polymerization. Then, the solution with the nPAM was polymerized by UV irradiation. For the removal of the nPAM included within the polymerized sample, the nPAM inside the polymer was exposed to 3.0 M sodium hydroxide aqueous solution for 48 h by the four-side open cutting. The cage-like PMMA template (CPT) was then fabricated to have a unique inverse pattern of the nPAM [20].

The CPT was dipped into lyotropic precursor solution in a vacuum condition and was rapidly stirred. The lyotropic precursor solution consisted of amphiphilic triblock copolymer (Pluronic F127; $EO_{106}PO_{70}EO_{106}$) and titanium (IV) isopropoxide of a titanium precursor in an acidic ethanol solution. The lyotropic precursor solution within the CPT was then allowed to be gellated at 60 °C for 12 h. Finally, the CPT was removed by chloroform solvent. The remaining product was calcinated at 450 °C for 12 h as the last process of the MTM fabrication.

2.3. Characterization of the MTM

The fabricated nPAM, CPT and MTM samples were characterized by using a field emission scanning electron microscope (FE-SEM, Hitachi, SU-70). High resolution transmission electron microscopy (HR-TEM, JEOL JEM-2100F) was also applied to determine the mesopore size, the particle size and the detailed structure of the MTM. The crystal phase of the MTM was investigated with x-ray diffractometry (XRD, PANalytical, X' Pert Pro MPD) working on Cu Kα radiation. The Brunauer–Emmett–Teller (BET) specific surface area of the MTM was determined by nitrogen adsorption measurement (Micromeritics ASAP-2010). Absorption and emission spectra were obtained with a diffuse reflectance UV–vis spectrophotometer (Jasco V-550) equipped with an integrating sphere (Jasco ISV-469), UV–vis spectrophotometer (Hitachi, U-2800) and spectrofluorometer (Hitachi, F-4500).

2.4. Photocatalytic degradation experiment

Photocatalytic decomposition of the rhodamine B (RhB) molecules in water solution was carried out in a 50 ml glass vessel with stirring. The reactor solutions were separately prepared by adding each 2.5 mg of the MTM and P25 (commercial Degussa TiO_2 particle) into two 20 ml of aqueous RhB solutions with the initial concentrations of 5.0×10^{-6} M. The MTM was immersed and fixed in the solution. Also P25 was suspended in the RhB solution with stirring. Before irradiation with UV light, the mixture solutions were magnetically stirred in the dark condition for 60 min to achieve an equilibrium state. UV light of 40 mW cm^{-2} was supplied by an Xe lamp (150 W, Abet Technologies, USA) equipped with a wide band reflection mirror that reflects the UV light in the wavelength range of 275–350 nm. During the photodecomposition experiment, the fluorescence spectrum of the remaining RhB molecules was measured to monitor the degree of photodissociation every 30 min.

2.5. Photovoltaic measurement

The dye-sensitized solar cell was fabricated as follows. The F-doped SnO_2 (FTO) conducting glass substrate (TEC8, Pilkington, 8 Ω/square, glass thickness of 2.3 mm) was

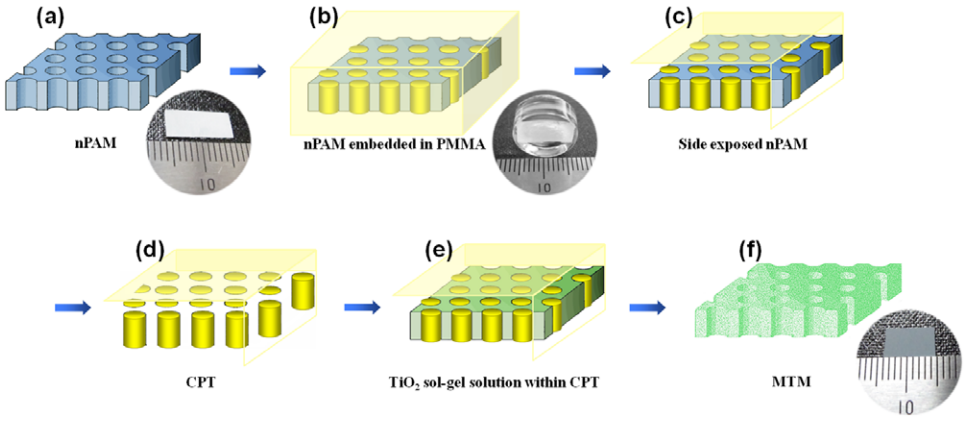

Figure 1. Schematic diagram for the fabrication process of the MTM. The round pictures represent the prepared materials.

ultrasonically pre-cleaned in ethanol. The fabricated MTM was then positioned on the FTO glass and dried in air at ambient temperature for 5 min. For the preparation with P25, a viscous paste was prepared as follows. A 0.2 g portion of ethyl cellulose, 0.05 g of lauric acid and 5 g of terpineol were added to an ethanol suspension containing 2.0 g of P25, and the solvent was then evaporated by a rotary evaporator at room temperature to obtain a viscous paste. The prepared P25 paste was coated on the bare FTO glass with the doctor blade method. The coated films were baked at 150 °C for 30 min.

The MTM and P25 with the FTO glasses were sintered at 500 °C for 30 min at a heating rate of 5 °C min^{-1}. The thicknesses of the annealed MTM and P25 were estimated to be 20 μm by an Alpha-step IQ surface profiler (KLA Tencor). For the dye adsorption, the annealed MTM and P25 with the FTO glass electrodes were immersed in the 0.5 mM dye solution of N719 dye (cis-di(thiocyanato)-*N*,*N*0-bis(2,20-bipyridyl-4-carboxylate-40-tetrabutyl ammonium carboxylate) Ru(II), Dyesol). The adsorption condition with the N719 dye solution was the same as the previous works reported [21, 22]. The Pt counter electrode was prepared as a film type by thermal reduction at 400 °C for 20 min with the 7 mM H_2PtCl_6 2-propanol solution. The dye-adsorbed MTM and P25 electrodes and the Pt counter electrode were sealed to be a sandwich type by using 60 μm-thick surlyn (Dupont 1702). The electrolyte solution in this system consisted of 0.7 M 1-butyl-3-methyl imidazolium iodide (PMII), 0.03 M I_2, 0.05 M guanidinium thiocyanate (GuSCN) and 0.5 M 4-tert-butylpyridine in a mixture solution of acetonitrile and valeronitrile (v/v 85:15). The active areas of the dye-adsorbed MTM film and the P25 film were estimated to be the same as 0.5 cm^2 by an image analysis program equipped with a digital microscope camera (Moticam 1000).

Photocurrent–voltage (I–V) measurements were performed using a Keithley model 2400 source measure unit. A class-A solar simulator (Newport) equipped with a 150 W Xe lamp was used as a light source, and the light intensity was adjusted with an NREL-calibrated Si solar cell with a KG-1 filter to approximate 1 sun light intensity. The photocurrent–voltage measurement of the dye-sensitized solar cells was performed with an aperture mask to prevent extra light coming through the lateral space according to a method proposed elsewhere [23].

3. Results and discussion

As illustrated in figure 1, the MTM was prepared by a two-step replication process. The CPT that had nanopillar arrays was firstly prepared by UV polymerization. Then, the mesoporous titania nanostructure with the membrane morphology was fabricated by introducing the TiO_2 sol–gel solution within the prepared CPT.

FE-SEM images of the fabricated nPAM are shown in figures 2(a) and (b). The pore diameter of the nPAM nanochannel is 250–300 nm at the applied voltage of 180 V in the H_3PO_4 electrolyte solution. Thickness of the fabricated nPAM is 60 μm. Figures 1(c) and (d) present FE-SEM images of the CPT prepared from the nPAM. The diameter of the nanowires and the thickness of the CPT are about 250 nm and 60 μm, respectively. It resembles the inverse structure of the utilized nPAM.

As shown in figures 3(a)–(d), the fabricated MTM has an ordered dual-pore structure. The primary nanoporous channel structure obtained from the duplication of the nPAM provides the porous membrane morphology with a nanochannel pore diameter of ∼300 nm (figures 3(a) and (b)). The interpore distance of the MTM is estimated to be 400–500 nm. These columnar nanochannels provide efficient diffusion pathway for the adsorption of the photocatalytic reactants and the dye molecules. Figures 3(c) and (d) reveal that the wall between the nanochannels has the secondary mesoporous structure formed by the sol–gel reaction of the lyotropic precursors. Also, the high magnification TEM image of the mesoporous wall indicates that the TiO_2 nanoparticles of about 10 nm in diameter form a mesoporous wall structure due to the controlled aggregation by the sol–gel reaction. This secondary mesoporous structure further maximizes the specific surface area of the MTM. Therefore, such dual-pore structure of the MTM improves the efficiencies of the photocatalytic activity and the DSSC compared with the powder packed form of P25. The HR-TEM image in the inset of figure 3(d) presents the single-crystalline nature of the nanocrystal which constructs

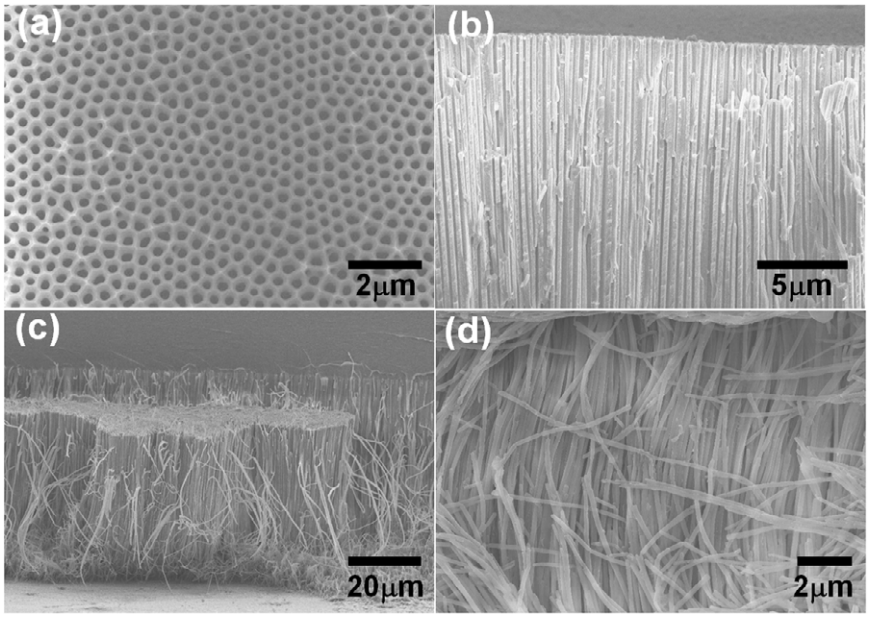

Figure 2. FE-SEM images of (a) top surface view of the nPAM, (b) cross-sectional view of the nPAM, (c) low magnification view of the CPT after removing the nPAM and (d) high magnification view of (c).

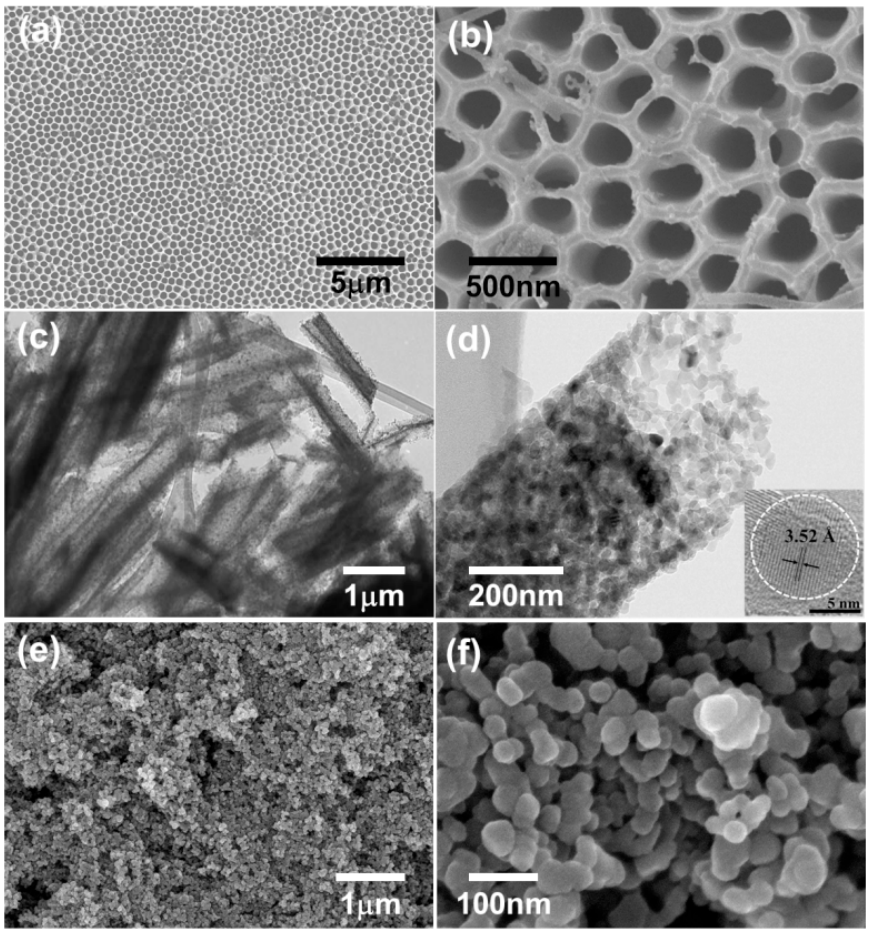

Figure 3. (a), (b) Low and high magnification FE-SEM images of the surface pore array, (c), (d) low and high magnification TEM images of the broken pieces of MTM. (e), (f) Low and high magnification FE-SEM images of the P25. Inset in (d) represents the HR-TEM image of a single TiO_2 nanoparticle of the tube wall.

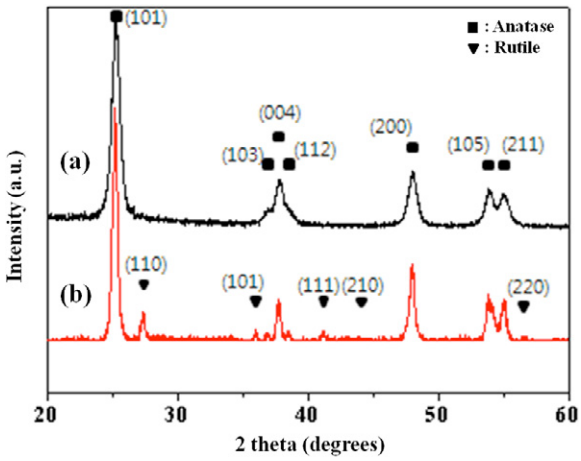

Figure 4. XRD patterns of (a) MTM and (b) P25.

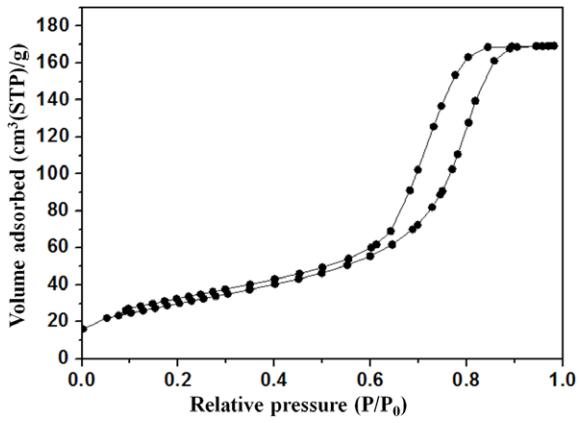

Figure 5. Nitrogen gas adsorption–desorption isotherm of the MTM.

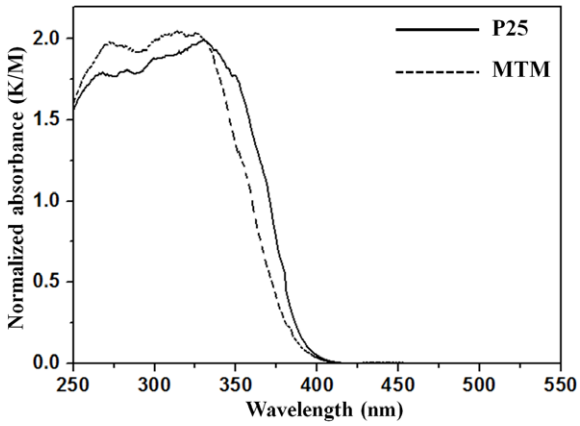

Figure 6. UV–vis diffuse reflectance absorption spectra of P25 and MTM.

the MTM. The distance between two neighboring planes is approximately 3.52 Å that is consistent with that of the (101) planes in the anatase structure of TiO_2. Figures 3(e) and (f) show FE-SEM images of P25. As shown in the figures, the P25 particles have irregular spherical shapes with a diameter range of 20–50 nm. These irregular spherical particles are piled together to form the packed structure. Compared with the dual-pore systems of MTM, this packed structure does not provide efficient channels for adsorption of the photocatalytic reactants and the dye molecules due to the random small pores among the P25 particles.

Figure 4 presents the XRD patterns of the MTM and P25. The XRD peaks of the MTM are relatively broader than the peaks of P25, which is ascribed to the smaller nanoparticle size of 10 nm compared with that of P25. However, the peak broadness of the MTM is still considered to be narrow due to the good crystalline phase. The strong Bragg reflection peaks ($2\theta = 25.3°$, 37.9°, 48.0°, 54.0° and 55.2°) are marked by the Miller indices ((101), (004), (200), (105) and (211)) from the diffraction data of anatase TiO_2 (JCPDS card no. 21-1272), which are the characteristic peaks of the anatase phase of the MTM. The crystalline size of the nanoparticles composing MTM is estimated by Scherrer's formula with the largest XRD peak at $2\theta = 25.3°$ [24, 25]. The estimated particle diameter is 12 nm, which is in good agreement with the crystalline size suggested from the TEM result. On the other hand, P25 is a TiO_2 composite that has a two-phase mixture of the anatase (70% in mass fraction) and rutile (30% in mass fraction) as reported in [26, 27].

The nitrogen gas adsorption–desorption isotherm data of figure 5 shows a unique hysteresis pattern that confirms the mesoporosity of the MTM. The BET specific surface area of the MTM is estimated to be 109.45 $m^2\ g^{-1}$, which is twice as large as that of P25 ($S_{BET} = 49.3\ m^2\ g^{-1}$) [25]. As mentioned above, the mesoporous framework is ascribed to this large S_{BET}.

The absorption spectra in figure 6 are obtained by applying the Kubelka–Munk function to the diffuse reflectance spectra. P25 shows the onset of its bandgap absorption at 395 nm that corresponds to 3.14 eV. The MTM exhibits characteristic absorption onset near the bulk bandgap (387 nm, 3.20 eV) of anatase titania.

The photocatalytic efficiency of the MTM is evaluated by the decomposition of RhB molecules under UV light irradiation in the wavelength range of 275–350 nm as shown in figure 7. The decomposition rates of RhB molecules in aqueous solution are monitored under the same experimental conditions for the MTM and P25 with 2.5 mg of each sample. The blank experiment without catalyst resulted in that RhB was not significantly decomposed only by the irradiation. Figure 7(b) indicates that the MTM has higher photocatalytic activity than P25 and the decomposition per cent of RhB is almost 100% at 120 min under the given conditions. The higher photocatalytic activity of the MTM is due to its characteristic morphology. As previously mentioned, P25 consists of 70% anatase phase and 30% rutile phase while the fabricated MTM only has the anatase phase. With respect to the different electro-hole recombination rates depending on the bandgap property, the anatase phase of titania is known to have higher photocatalytic activity than the rutile [28–30]. In addition, the surface quantum effect offers more active sites, upon irradiation by light, to the water molecules for the redox reaction that generates reactive oxygen species including the hydroxyl radicals which oxidize the RhB molecules [31].

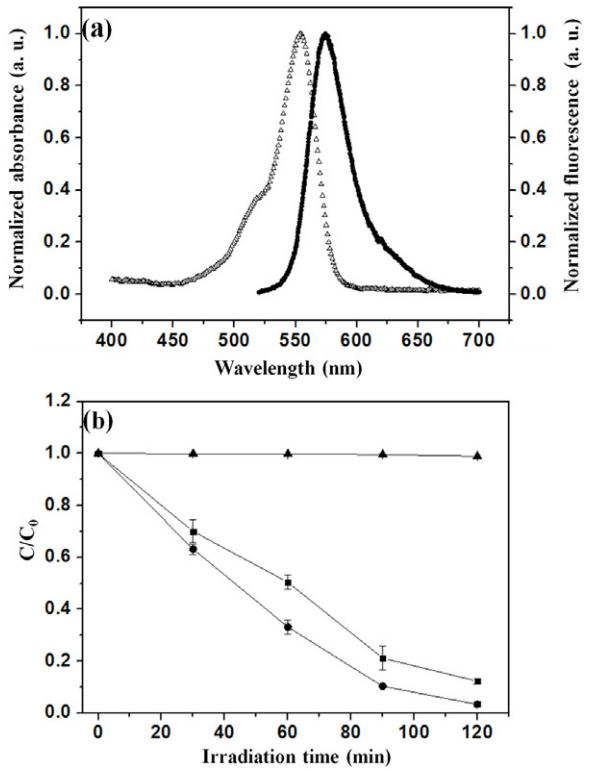

Figure 7. (a) Steady-state absorption (—△—) and fluorescence (—●—) spectra of RhB in aqueous solution. (b) Decomposition ratio of RhB as a function of the irradiation time for the RhB solution only under the UV light (—▲—), the decomposition ratio with P25 under UV light (—■—) and the decomposition ratio with the MTM under UV light (—●—). The decomposition ratio was estimated by the emission intensity of the RhB solution at 577 nm with an excitation of 550 nm.

Therefore, the MTM shows better photocatalytic activity than P25 does.

Since MTM has the morphology of the membrane-type film with a dual-pore structure, its application to a dye-sensitized solar cell is preliminarily tried. As shown in figure 8, the photovoltaic performance of the MTM DSSC was compared to that of P25. The open-circuit voltage, a short-circuit current density, the fill factor and solar energy conversion efficiency of the reference cell of P25 were estimated as 0.88 V, 4.72 mA cm^{-2}, 0.73 and 3.03%, respectively. On the other hand, the dye-sensitized solar cell assembled with the MTM resulted in 0.84 V, 5.32 mA cm^{-2}, 0.75 and 3.35% for the corresponding factors as above. The MTM cell fabricated in this study clearly indicates better solar energy conversion efficiency for its DSSC application than the standard P25 does.

A major factor for this advantage is that the unique structure of the MTM. The fabricated MTM has the ordered dual-pore structure. The primary nanoporous channel structure obtained from the duplication of the nanoporous alumina membrane provides the porous membrane morphology with the nanochannel pore diameter of ∼300 nm (figures 3(a) and (b)). These columnar nanochannels provide an efficient diffusion pathway for the adsorption of the dye molecules. In

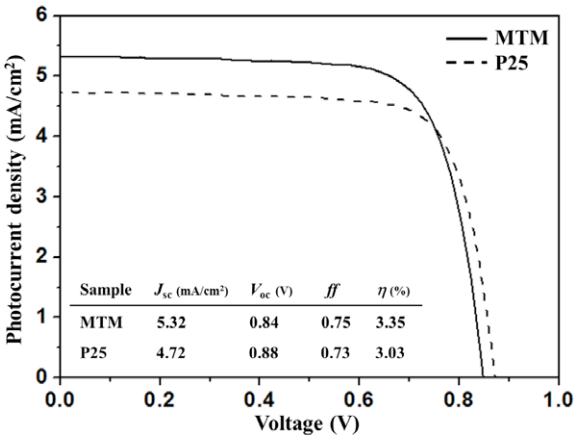

Figure 8. The photocurrent–voltage characteristic of the dye-sensitized solar cell fabricated with the MTM and P25.

addition, the secondary mesoporous structure further enhances the adsorption of the dye molecules by maximizing the specific surface area of the MTM. Therefore, the MTM with ordered dual-pore structure provides a higher photovoltaic performance compared with P25 due to better dye adsorption [32, 33]. Another factor for this better DSSC efficiency is the good contact amongst the nanoparticles that form the nanochannel wall of the MTM, as shown in figure 3(d). These interconnected nanoparticles increase the interface coupling cross sections that result in the increase of the electron transfer efficiency throughout the MTM [34, 35].

4. Conclusions

In summary, the MTM with a well-ordered dual-pore array is synthesized by a two-step replication process. The dual-pore array consists of mesoporous nanopores (∼5 nm) and straight nanochannels of 300 nm in pore diameter within the membrane frame. Such a dual-pore pattern of the MTM provides a large surface area of $S_{BET} = 109.45\ m^2\ g^{-1}$. The large surface area and the anatase structure of 100% result in the high photocatalytic activity compared with P25 and the solar energy conversion efficiency of 3.35% for the dye-sensitized solar cell system as a preliminary test. The successful fabrication demonstration of the large size MTM with a nano-dual-pore array by a two-step replication method can be further applied to highly efficient recyclable catalyst, membrane solar cells, etc.

Acknowledgments

This study was supported by a grant of the Korea Healthcare Technology R&D Project, Ministry for Health, Welfare & Family Affairs, Republic of Korea (grant no. A085136) and the KOSEF through the Pioneer Converging Technology Program (grant no. 2010-0002190). KK is grateful for the grant from the New and Renewable Energy Program through the Korea Institute of Energy Technology Evaluation and Planning (KETEP) funded by the Ministry of Knowledge Economy (MKE).

References

[1] Onoda K and Yoshikawa S 2008 *Appl. Catal.* B **80** 277
[2] Sauvage F, Fonzo F D, Bassi A L, Casari C S, Russo V, Divitini G, Ducati C, Bottani E C, Comte P and Graetzel M 2010 *Nano Lett.* **10** 2562
[3] Nam W, Oh S, Joo H, Sarp S, Cho J, Nam B-W and Yoon J 2010 *J. Sol. Energy Mater. Sol. Cell* **94** 1809
[4] Son M-S, Im J-E, Wang K-K, Oh S-L, Kim Y-R and Yoo K-H 2010 *Appl. Phys. Lett.* **96** 23115
[5] Topoglidis E, Campbell C J, Cass A E G and Durrant J R 2001 *Langmuir* **17** 7899
[6] Zhao D, Chen C, Wang Y, Ma W, Zhao J, Rajh T and Zang L 2008 *Environ. Sci. Technol.* **42** 308
[7] Jiang D, Zhang S and Zhao H 2007 *Environ. Sci. Technol.* **41** 303
[8] Kamat P V 2007 *J. Phys. Chem.* C **111** 2834
[9] Lee G-W, Kim D, Ko M J, Kim K and Park N-G 2010 *Sol. Energy* **84** 418
[10] Choi H, Sofranko A C and Dionysiou D D 2006 *Adv. Funct. Mater.* **16** 1067
[11] Yu J, Zhang L, Cheng B and Su Y 2007 *J. Phys. Chem.* C **111** 10582
[12] Pookmanee P and Phanichphant S 2009 *J. Ceram. Process. Res.* **10** 167
[13] Nam H-J, Amemiya T, Murabayashi M and Itoh K 2004 *J. Phys. Chem.* B **108** 8254
[14] Liu H, Cheng S, Zhang J and Cao C 1999 *Chemosphere* **38** 283
[15] Neppolian B, Kanel S R, Choi H C, Shankar M V, Araninodoo B and Murugesan V 2003 *Int. J. Photoenergy* **5** 45
[16] Kwon J M, Kim Y H, Song B K, Yeom S H, Kim B S and Im J B 2006 *J. Hazard. Mater.* **134** 230
[17] Shin Y and Lee S 2008 *Nano Lett.* **8** 3171
[18] Choi J, Wehrspohn R B, Lee J and Gösele U 2004 *Electrochim. Acta* **49** 2645
[19] Masuda H, Yada K and Osaka A 1998 *Japan. J. Appl. Phys.* **37** L1340
[20] Yanagishita T, Nishio K and Masuda H 2005 *Adv. Mater.* **17** 2241
[21] Hwang S *et al* 2007 *Chem. Commun.* 4887
[22] Lee K, Park S W, Ko M J, Kim K and Park N-G 2009 *Nat. Mater.* **8** 665
[23] Park J, Koo H-J, Yoo B, Yoo K, Kim K, Choi W and Park N-G 2007 *Sol. Energy Mater. Sol. Cells* **91** 1749
[24] Reyes-Coronado D, Rodriguez-Gattorno G, Espinosa-Pesqueira M E, Cab C, Coss R and Oskam G 2008 *Nanotechnology* **19** 145605
[25] Wang Y, Zhang L, Deng K, Chen X and Zou Z 2007 *J. Phys. Chem.* C **111** 2709
[26] Yu J, Yu H, Cheng B, Zhou M and Zhao X 2006 *J. Mol. Catal.* A **253** 112
[27] Pavasupree S, Jitputti J, Ngamsinlapasathian S and Yoshikawa S 2008 *Mater. Res. Bull.* **43** 149
[28] Wu N, Wang J, Tafen D N, Wang H, Zheng J-G, Lewis J P, Liu X, Leonard S S and Manivannan A 2010 *J. Am. Chem. Soc.* **132** 6679
[29] Baiju K V, Shukla S, Sandhya K S, James J and Warrier K G K 2007 *J. Phys. Chem.* C **111** 7612
[30] Cavigli L, Bogani F, Vinattieri A, Cortese L, Colocci M, Faso V and Baldi G 2010 *Solid State Sci.* **12** 1877
[31] Wu S and He J 2011 *J. Mater. Chem.* **21** 2852
[32] Orilall M C and Wiesner U 2011 *Chem. Soc. Rev.* **40** 520
[33] Qian J, Liu P and Cao Y 2009 *Adv. Mater.* **21** 3663
[34] Wu C and Wu J 2011 *J. Mater. Chem.* **21** 2871
[35] Lee S, Lee J, Jung H S and Hong K S 2010 *Chem. Mater.* **22** 1958